https://doi.org/10.5194/wes-2025-70
Preprint. Discussion started: 5 May 2025

eawe european academy of wind energy
Open Access WIND ENERGY SCIENCE DISCUSSIONS

Load models for tapered roller bearings and influence of system deformation —— taking the main bearing system of wind turbines as an example

Xuehai Gao[1,+,*], Sizhe Ren[1], Zekun Zhang[2], Xiao-Jing Guo[3,*]
[1]School of Mechanical Engineering, Shanghai Dianji University, Shanghai 201306, People's Republic of China
[2]Kaiserslautern Intelligent Manufacturing School, Shanghai Dianji University, Shanghai 201306, People's Republic of China
[3]The Education Ministry Key Laboratory of Resource Chemistry, Shanghai Key Laboratory of Rare Earth Functional Materials, Department of Chemistry and Chemical Engineering, Shanghai Normal University, 100 Guilin Road, Shanghai, 200234, People's Republic of China

Correspondence to: Xuehai Gao (xuehai_gao84@163.com); Xiao-Jing Guo (guoxj@shnu.edu.cn)

Abstract. Firstly, a tapered roller bearing (TRB) raceway contact load model is developed based on the rigid assumption of the bearing system, taking a wind turbine TRB+TRB main bearing system as an example. Then, a simplified TRB FEA modeled is presented considering the deformation of the bearing system. The FEA model makes the simulation of complex bearing system more feasible and efficient, avoiding the challenges of meshing and convergence in rollers and raceway contact modeling. A two-step method is proposed to take difference of outer and inner raceway contact angles into consideration. The FEA modeled is validated by comparing its results with those of a solid elements roller model. Subsequently, the FEA model is used to simulate the wind turbine TRB+TRB main bearing system, and results of FEA model and rigid model are compared to demonstrate the influence of the bearing system deformation. The results shows the bearing system deformation has an obvious influence on TRB raceway load distribution and roller profile modification, and the developed models are efficient to assess the influence.

Keywords. finite element analysis, tapered roller bearing, wind turbine

1 Introduction

Increasingly, engineering failures and research have shown that the deformation of the entire bearing system significantly affects the performance of large-sized bearings (Krynke et al., 2011; Stammler et al., 2024). It notably differs from traditional bearing design guidelines, which are based on Hertz's theory, such as ISO 76 and ISO 281. The bearing rings are assumed to be rigid, and the only deformation is caused by roller and raceway contact in these design guidelines.

The solid elements roller model is a straightforward solution that comes to mind. However, it presents challenges in terms of meshing, roller boundary setting, convergence, and CPU time. To be efficiently utilized in complex engineering practices, a

https://doi.org/10.5194/wes-2025-70
Preprint. Discussion started: 5 May 2025

eawe european academy of wind energy
Open Access WIND ENERGY SCIENCE DISCUSSIONS

bearing simplification modeling method has been proposed. Ruben et al (Lostado-Lorza et al., 2017) developed a method combining FEA with data mining technology. This method learns 81 FEA results of different work conditions through machine learning technology to establish the response of bearings under different work conditions, then explore the bearing optimization. Rollers are modeled by solid elements. This method is applicable to bearing system with similar topological structure, which lacks general applicability. Some works establish the force balance equation for rollers and external loads to determine the raceway load distribution, and subsequently create a sector model of the roller and raceway contact region (Lostado et al., 2015; Safian et al., 2021; Yongqi et al., 2012). However, this approach overlooks the impact of bearing system deformation on raceway load, which is particularly significant for large bearing systems. Some researchers model TRB rollers using only compressive truss elements, a method that neglects the nonlinear behavior in the compression zone and the connection nodes of the bearing, as well as the difference in contact angles between the inner and outer raceways (Nie et al., 2023).

In recent years, spring-based element has been more and more used in huge bearing FEA works including ball bearings (X. H. Gao et al., 2011; Liu et al., 2018; Stammler et al., 2024), cylinder roller bearings (CRB) (He et al., 2021), spherical roller bearings (SRB) (X. Gao & Zhang, 2024) and wire race bearings (Gunia & Smolnicki, 2017).

Regarding a TRB, the contact angles of the outer and inner raceways differ, indicating that the raceways cannot be connected by a single set of springs perpendicular to both. Furthermore, the contact between the inner ring flange and the roller ends must be taken into account. These factors complicate the direct simulation of TRB performance with high efficiency in a single step. In this paper, we propose a technique for modeling TRB bearings using nonlinear springs, which accounts for the complex roller-raceway contact geometry. This serves as a reference method for evaluating and optimizing TRB performance under the deformation of the entire bearing system. Additionally, a practical engineering case involving a wind turbine main bearing system is used to demonstrate the application of the developed model.

2 TRB loads based on traditional rigid system assumption

The inner and outer rings of a TRB bearing are separable and must be used in pairs in engineering applications. Fig. 1(a) shows a typical TRB + TRB wind turbine main bearing system. The bearing closer to the wind turbine rotor is usually called the front bearing (FB), and the bearing closer to the gearbox is usually called the rear bearing (RB). To ensure the performance of the bearings, the bearings usually be pre-tightened with a clamping ring as shown in Fig. 1 (b). The clamping amount is presented by S in the paper. In the assumption of a rigid model, the overall structure of the system remains rigid, and only Hertz contact deformation occurs in the contact area between the rolling elements and the raceways.

The system can be simplified as Fig. 2 without considering the deformation of main bearing and bearing housing. The radial loads acting on FB and RB can be obtained using Eq. (1) when the hub center load is applied as shown in Fig. 3.

https://doi.org/10.5194/wes-2025-70
Preprint. Discussion started: 5 May 2025

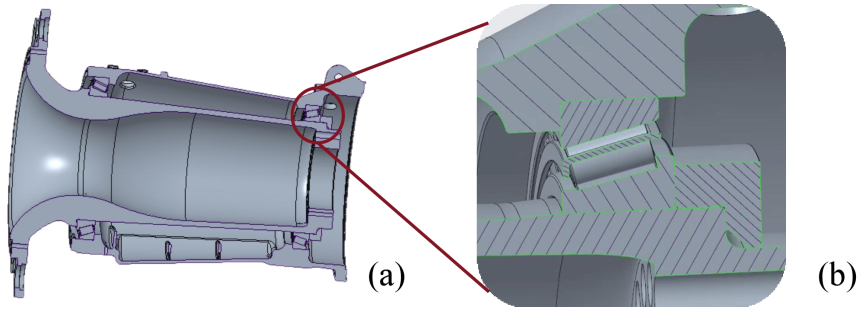

Fig 1. TRB+TRB wind turbine main bearing system: (a) section view; (b) scaled view of pre-tightening structure.

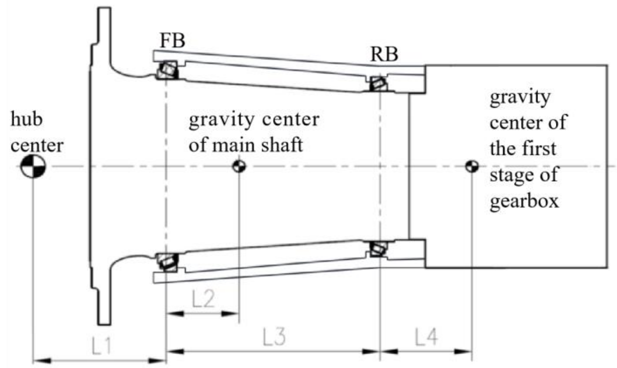

Fig. 2 The simplification of the bearing system

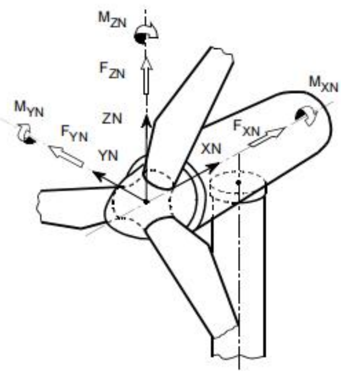

Fig. 3 Hub center loads (Germanischer Lloyd, 2010)

$$\begin{bmatrix} F_{\mathrm{YFB}} \\ F_{\mathrm{ZFB}} \\ F_{\mathrm{YRB}} \\ F_{\mathrm{ZRB}} \end{bmatrix} \begin{bmatrix} 1 & 0 & 1 & 0 \\ 0 & 1 & 0 & 1 \\ 0 & L_1 & 0 & L_1+L_3 \\ L_1 & 0 & L_1+L_3 & 0 \end{bmatrix} = \begin{bmatrix} -F_{\mathrm{YN}} \\ -F_{\mathrm{ZN}}+G_{\mathrm{MS}}+G_{\mathrm{GBX}} \\ M_{\mathrm{YN}}+(L_1+L_2)G_{\mathrm{MS}}+(L_1+L_3+L_4)G_{\mathrm{GBX1st}} \\ -M_{\mathrm{ZN}} \end{bmatrix} \tag{1}$$

where, F_{Y}: bearing loads in the Y direction, with subscripts FB and RB representing FB and RB respectively; F_{Z}: bearing loads in the Z direction, with subscripts FB and RB representing FB and RB respectively; G_{MS}: gravity of main shaft; G_{GBX}: gravity of the first stage of gearbox.

It is noted that the axial load of bearings can not be obtained directly from the equation of the force equilibrium with hub center loads. The pre-tightening alters the axial load shearing between FB and RB. Eqs (2-6) are used to calculate the axial loads, taking into account the pre-tightening.

$$S_{\mathrm{FB}}+S_{\mathrm{RB}}=S \tag{2}$$

$$Z_{\mathrm{FB}}C_{\mathrm{LFB}}\left(S_{\mathrm{FB}}\sin\alpha_{\mathrm{OFB}}\right)^{10/9}\sin\alpha_{\mathrm{OFB}}-Z_{\mathrm{RB}}C_{\mathrm{LRB}}\left(S_{\mathrm{RB}}\sin\alpha_{\mathrm{ORB}}\right)^{10/9}\sin\alpha_{\mathrm{OFB}}=0 \tag{3}$$

$$F_{\mathrm{XFB}}+F_{\mathrm{XRB}}=F_{\mathrm{XN}} \tag{4}$$

$$\begin{aligned} &F_{\mathrm{XFB}}=Z_{\mathrm{FB}}C_{\mathrm{LFB}}\left(\left(S_{\mathrm{FB}}+\delta_{\mathrm{X}}\right)\sin\alpha_{\mathrm{OFB}}\right)^{10/9}\sin\alpha_{\mathrm{OFB}}, \quad S_{\mathrm{FB}}+\delta_{\mathrm{X}}>0 \\ &F_{\mathrm{XFB}}=0, \quad S_{\mathrm{FB}}+\delta_{\mathrm{X}}\le 0 \end{aligned} \tag{5}$$

https://doi.org/10.5194/wes-2025-70
Preprint. Discussion started: 5 May 2025

$$
\begin{aligned}
&F_{\mathrm{XRB}} = Z_{\mathrm{RB}} C_{\mathrm{LRB}} \left((S_{\mathrm{RB}} - \delta_{\mathrm{X}}) \sin \alpha_{\mathrm{ORB}} \right)^{10/9} \sin \alpha_{\mathrm{ORB}}, \qquad S_{\mathrm{RB}} - \delta_{\mathrm{X}} > 0 \\
&F_{\mathrm{XRB}} = 0, \qquad S_{\mathrm{RB}} - \delta_{\mathrm{X}} \le 0
\end{aligned} \tag{6}
$$

where, S: total pre-tightening amount, with subscripts FB and RB representing FB and RB respectively; Z: number of rollers, with subscripts FB and RB representing FB and RB respectively; C_{L}: spring constant according to ISO16281, with subscripts FB and RB representing FB and RB respectively; α_0: bearing contact angle, with subscripts FB and RB representing FB and RB respectively; F_{X}: axial loads acting on bearings, with subscripts FB and RB representing FB and RB respectively; δ_{X}: main shaft displacement under axial load from hub center (F_{XN}).

The external loads acting on FB and RB can be determined by Eqs. (1-6). In order to assess the performance of bearings, it is necessary to solve the raceway contact load distribution or loads acting on each roller. Fig. 4 illustrates the response when the external loads act on a TRB. When F_{Y} and F_{Z} act on a TRB in the radial plane, a radial relative displacement (δ_{r}) between bearing rings occurs. Assuming the angle between δ_{r} and Z direction is θ, and ϕ_i represents the circular position of the ith roller relative to δ_{r} direction. The axial load F_{X} causes relative displacement δ_{a} in axial direction. δ_{r}, δ_{a} and θ can be calculated by Eq. (7), and then the contact load between outer raceway and rollers.

$$
\begin{bmatrix}
\sum_{i=1}^{Z_{\mathrm{FB}}} C_{\mathrm{LFB}} \left(\delta_{\mathrm{rFB}} \cos \phi_{i\mathrm{FB}} \cos \alpha_{\mathrm{OFB}} + \delta_{\mathrm{aFB}} \sin \alpha_{\mathrm{OFB}} \right)^{10/9} \sin \alpha_{\mathrm{OFB}} \\
\sum_{i=1}^{Z_{\mathrm{FB}}} C_{\mathrm{LFB}} \left(\delta_{\mathrm{rFB}} \cos \phi_{i\mathrm{FB}} \cos \alpha_{\mathrm{OFB}} + \delta_{\mathrm{aFB}} \sin \alpha_{\mathrm{OFB}} \right)^{10/9} \cos(\theta_{\mathrm{FB}} + \phi_{i\mathrm{FB}}) \cos \alpha_{\mathrm{OFB}} \\
\sum_{i=1}^{Z_{\mathrm{FB}}} C_{\mathrm{LFB}} \left(\delta_{\mathrm{rFB}} \cos \phi_{i\mathrm{FB}} \cos \alpha_{\mathrm{OFB}} + \delta_{\mathrm{aFB}} \sin \alpha_{\mathrm{OFB}} \right)^{10/9} \sin(\theta_{\mathrm{FB}} + \phi_{i\mathrm{FB}}) \cos \alpha_{\mathrm{OFB}} \\
\sum_{i=1}^{Z_{\mathrm{RB}}} C_{\mathrm{LRB}} \left(\delta_{\mathrm{rRB}} \cos \phi_{i\mathrm{RB}} \cos \alpha_{\mathrm{ORB}} + \delta_{\mathrm{aRB}} \sin \alpha_{\mathrm{ORB}} \right)^{10/9} \sin \alpha_{\mathrm{ORB}} \\
\sum_{i=1}^{Z_{\mathrm{RB}}} C_{\mathrm{LRB}} \left(\delta_{\mathrm{rRB}} \cos \phi_{i\mathrm{RB}} \cos \alpha_{\mathrm{ORB}} + \delta_{\mathrm{aRB}} \sin \alpha_{\mathrm{ORB}} \right)^{10/9} \cos(\theta_{\mathrm{RB}} + \phi_{i\mathrm{RB}}) \cos \alpha_{\mathrm{ORB}} \\
\sum_{i=1}^{Z_{\mathrm{RB}}} C_{\mathrm{LRB}} \left(\delta_{\mathrm{rRB}} \cos \phi_{i\mathrm{RB}} \cos \alpha_{\mathrm{ORB}} + \delta_{\mathrm{aRB}} \sin \alpha_{\mathrm{ORB}} \right)^{10/9} \sin(\theta_{\mathrm{RB}} + \phi_{i\mathrm{RB}}) \cos \alpha_{\mathrm{ORB}}
\end{bmatrix}
=
\begin{bmatrix}
F_{\mathrm{XFB}} \\ F_{\mathrm{ZFB}} \\ F_{\mathrm{YFB}} \\ F_{\mathrm{XRB}} \\ F_{\mathrm{ZRB}} \\ F_{\mathrm{YRB}}
\end{bmatrix} \tag{7}
$$

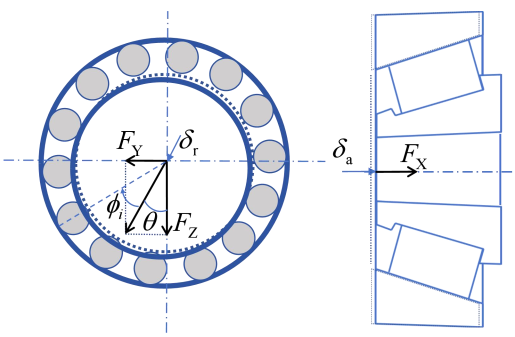

Fig. 4 Response when the external loads act on a TRB

https://doi.org/10.5194/wes-2025-70
Preprint. Discussion started: 5 May 2025

3 FEA Modelling of a TRB

3.1. TRB model description

Fig. 5(a) depicts the typical geometry of a TRB raceway and the relationship among the contact loads. The usually called bearing contact angle is actually the outer raceway contact angle (α_{O}), α_{I} represents the inner raceway contact angle, α_{F} represents the inner ring flange angle, and α_{R} represents the roller cone angle. Different from common CRBs, for TRBs, $\alpha_{\mathrm{O}} \neq \alpha_{\mathrm{I}}$ and $\alpha_{\mathrm{F}} \neq 90°$, so the contact loads acting on the outer raceway (Q_{O}) and on the inner raceway (Q_{IR}) are not collinear. The load acting on the inner ring (Q_{I}) which is in the opposite direction and has the same magnitude as Q_{O} should be the resultant of Q_{IR} and contact load acting on the inner ring flange (Q_{IF}). The relationships among these loads are expressed by Eqs (1-2), in which the friction on the raceways and the flange is neglected.

$$Q_{\mathrm{IR}} \cos \alpha_{\mathrm{I}} + Q_{\mathrm{IF}} \cos(\alpha_{\mathrm{IF}} - \alpha_{\mathrm{I}}) - Q_{\mathrm{O}} \cos \alpha_{\mathrm{O}} = 0 \tag{8}$$

$$Q_{\mathrm{IR}} \sin \alpha_{\mathrm{I}} + Q_{\mathrm{IF}} \sin(\alpha_{\mathrm{IF}} - \alpha_{\mathrm{I}}) - Q_{\mathrm{O}} \sin \alpha_{\mathrm{O}} = 0 \tag{9}$$

To simulate a bearing using springs, the springs should be oriented in the direction of the raceway contact load. However, the contact loads acting on the outer and inner raceways are in different directions. This implies that it is not feasible to model a TRB while simultaneously obtaining the contact loads Q_{O}, Q_{IR} and Q_{IF}. This is also a key challenge in TRB modelling compared to CRB modelling. A two-step method is developed to account for the different contact angles.

Step 1: modelling TRB with springs to obtain Q_{O}. There is only Q_{O} load between the roller and outer ring, and it is perpendicular to the outer raceway. Consequently, it can be modeled using a set of springs, as illustrated in Fig. 5(b). The spring nodes adjacent to the outer raceway are rigidly tied to the neighboring area of the outer raceway, and the nodes near the inner raceway are rigidly tied to the neighboring area of the inner raceway. The sum of the spring loads is equal to Q_{O}. The modeling process using the commercial software ABAQUS is shown in Fig. 5(c). It is recommended that the width of the tied regions on the outer and inner raceways be approximately 10% of the roller diameter.

Step 2: calculating Q_{IR} and Q_{IF}. Since Q_{O} is obtained in step 1, Q_{IR} and Q_{IF} can be calculated according to Eqs (8-9).

A roller is modeled using 3 springs in the paper. We have investigated the influence of the number of springs on the simulation results in a roller-raceway contact. It was found that when the number of springs exceeds 2, there is no significant difference in the simulation results (Wang et al., 2017). Therefore, this aspect will not be discussed further in the paper. According to Hertz contact theory, the relationship between the line contact load and deformation can be expressed as Eq. (10) (Tedric A. Harris & Kotzalas, 不详-b). In a TRB, line contact occurs on both the outer and inner raceways. Thus, the spring stiffness should be approximately half of the value of a single contact pair, as shown in Eq. (11).

$$\delta = 3.84 \times 10^{-5} \frac{Q^{0.9}}{L_{\mathrm{we}}^{0.8}} \tag{10}$$

$$\delta_{\mathrm{s}} = 2 \times 3.84 \times 10^{-5} \frac{Q^{0.9}}{(L_{\mathrm{we}}/n_{\mathrm{s}})^{0.8}} \tag{11}$$

https://doi.org/10.5194/wes-2025-70
Preprint. Discussion started: 5 May 2025

where, δ: contact deformation of a single line contact pair (mm); L_{we}: effective roller length (mm); Q: roller-raceway contact load (N); n_s: number of springs in a roller-raceway contact modeling (mm); δ_s: spring deformation (mm).

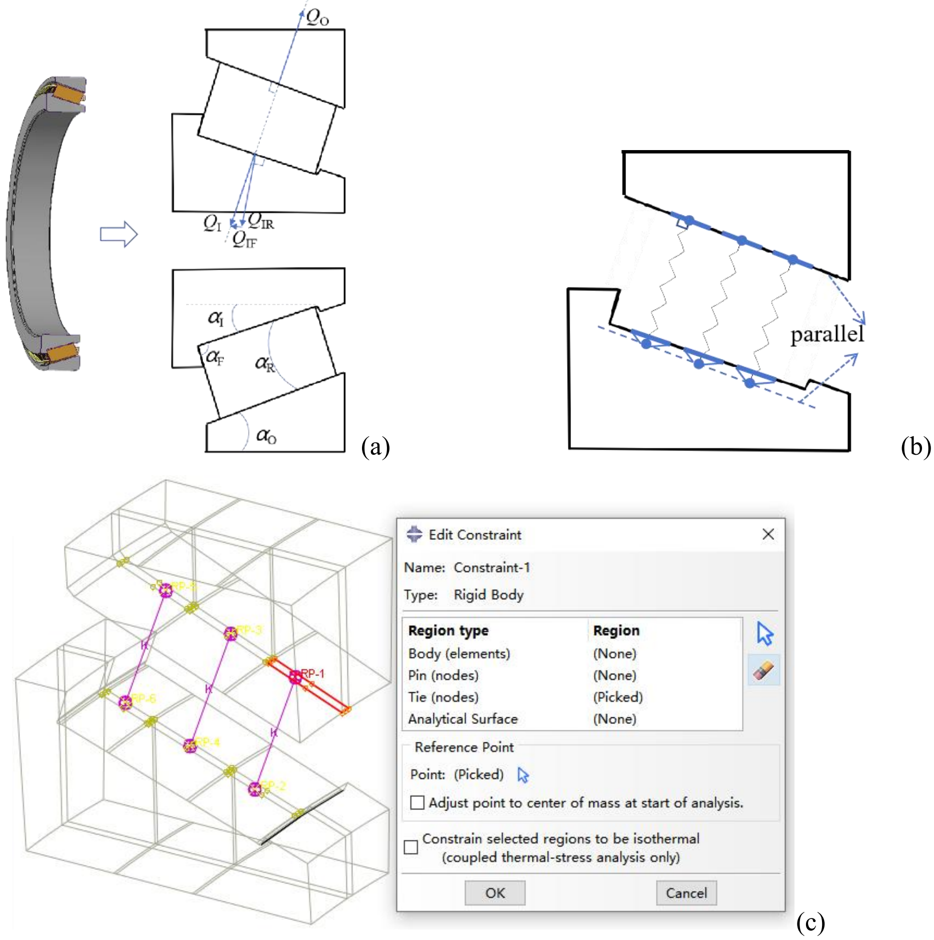

120 **Fig 5. Model depiction: (a) TRB geometry and contact load; (b) TRB modeling schematic; (c) an example of modeling process in ABAQUS.**

3.2. Model validation

A wind turbine main bearing system is utilized to validate the proposed FEA model and demonstrate its practical application, and key parameters of FB and RB are presented in Table 1.

125 Table 1. Parameters of bearings

Items	FB (TRB1500)	RB (TRB1350)
inner diameter I.D. mm	1500	1350
outer diameter O.D. mm	1965	1740
bearing thickness T mm	220	190

https://doi.org/10.5194/wes-2025-70
Preprint. Discussion started: 5 May 2025

outer ring thickness O.T. mm	175	165
inner ring thickness I.T. mm	220	190
number of rollers Z	52	57
contact angle α_0 °	21	15
roller length L_{we} mm	160	140
roller diameter D_{we} mm	96.4	80.5
inner raceway contact angle α_{I} °	18.9	13.6
inner flange angle α_{F} °	89.76	89.84

To validate the model, a one-roller sector of the front bearing was modeled using solid elements for the roller and spring elements, as shown in Fig. 6. The model and its boundary conditions are detailed in Table 2.

The deformation results at the last load step are compared as shown in Fig. 7. Reaction forces at reference points are extracted to validate the model. The results in Fig. 8 indicate that the outcomes of the spring model are in excellent agreement with those of the solid elements model. Regarding the solving time, the solid elements roller model consumed 37539s CPU time, while the spring model only took 103.7s using the same computer and solving configuration.

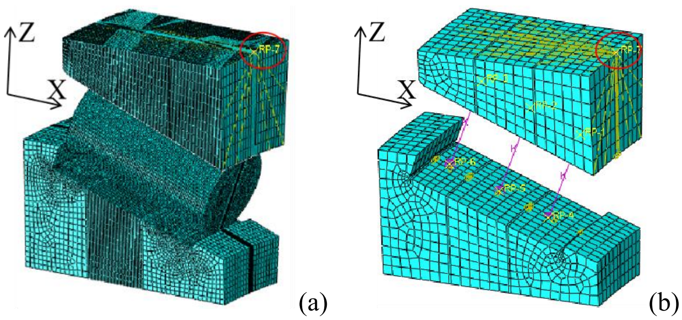

Fig 6. FEA model of a roller-sector of TRB: (a) solid elements roller; (b) spring elements model.

Table 2. Validation model details

Items	Model with Solid Elements Roller	Model with Spring elements
Mesh	411856 8-nodes linear brick with incompatible modes elements Contact region elements size: 1.5 × 0.3mm	4862 8-nodes linear brick with incompatible modes elements + 3 spring elements
Material	Steel with Yang’s modulus 210000MPa and Poisson's ratio 0.3	
Interaction	3 contact pairs: roller-outer raceway, roller-inner raceway and roller-inner flange; contact property: frictionless surface to surface hard contact	3 spring elements be modeled according to Fig. 1(c).
	Reference points in red circles shown in Fig. 3 are coupled to outer ring on outer diameter and end face. The displacement is applied on the reference points.	

https://doi.org/10.5194/wes-2025-70
Preprint. Discussion started: 5 May 2025

Boundary Conditions	The inner diameter face of inner ring is fixed. -0.1mm in X direction and -0.3 in Z direction is applied by 10 equally spaced steps.

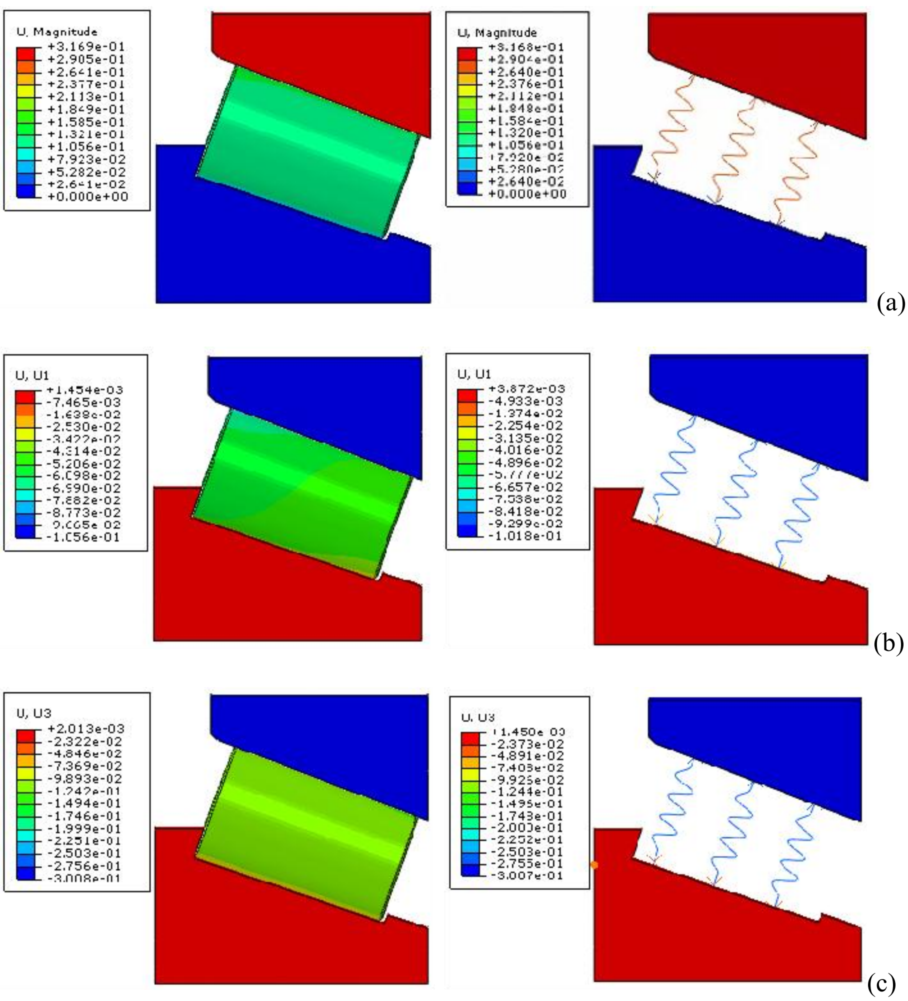

Fig 7. Deformation results comparison at the last load step: (a) deformation magnitude; (b) deformation in X direction; (c) deformation in Z direction.

https://doi.org/10.5194/wes-2025-70
Preprint. Discussion started: 5 May 2025

eawe european academy of wind energy
Open Access
WIND ENERGY SCIENCE DISCUSSIONS

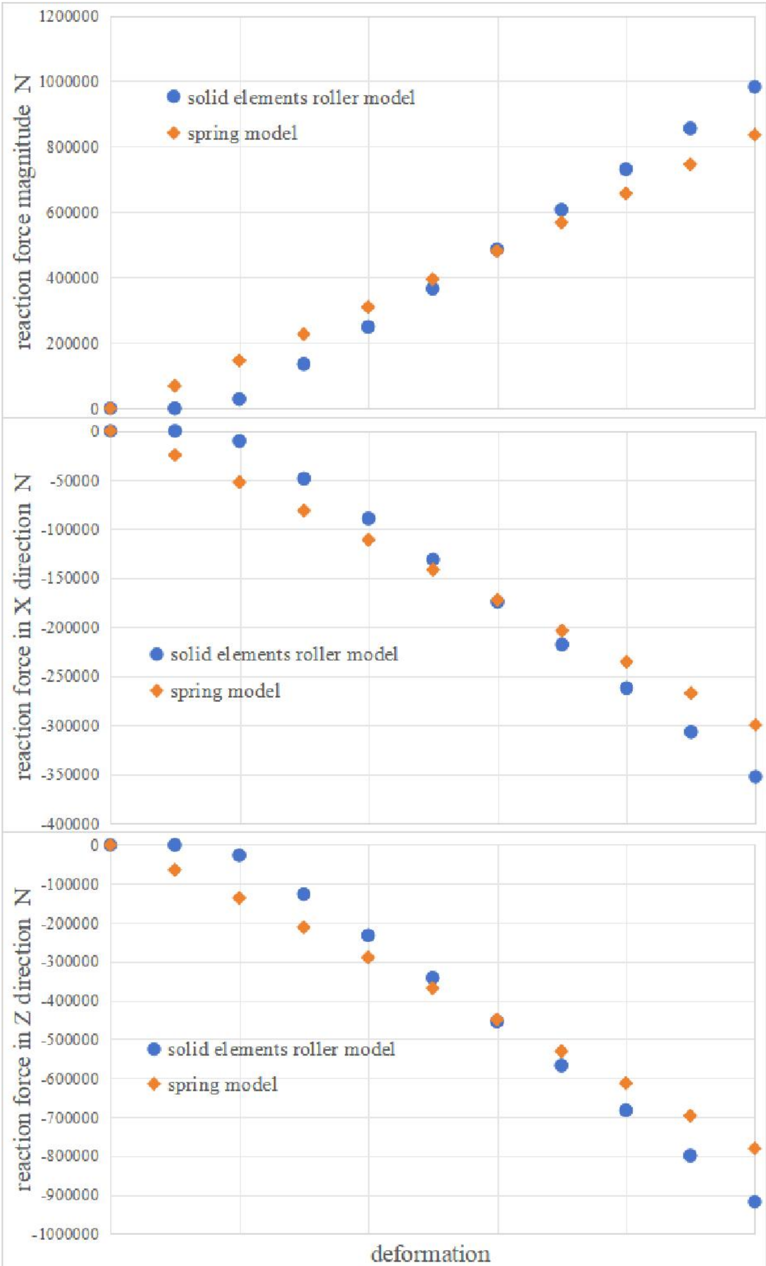

X(mm)	0	-0.01	-0.02	-0.03	-0.04	-0.05	-0.06	-0.07	-0.08	-0.09	-0.1
Z(mm)	0	-0.03	-0.06	-0.09	-0.12	-0.15	-0.18	-0.21	-0.24	-0.27	-0.3

Fig 8. Model validation with reaction forces

https://doi.org/10.5194/wes-2025-70
Preprint. Discussion started: 5 May 2025

4 Engineering application of the model

4.1 Model description

Fig. 9(a) presents the FEA model of the wind turbine main bearing system, while TRB models are depicted in Fig. 9(b). Reference point “RP-load” is at the hub center and coupled to the main shaft hub side end face to apply hub center load. Reference point “RP-Shaft” is at the gravity center of main shaft and coupled to main shaft to apply the main shaft gravity. Reference point “GBX1st” is at the gravity center of the first stage of gearbox and coupled to main shaft gearbox side end face to apply the first stage of gearbox gravity. Reference point “GBX” is at the gravity center of the gearbox and coupled to main bearing housing gearbox end face to apply the gearbox gravity. Interactions between TRBs, main shaft, bearing housing and preload ring are defined as hard contacts with a friction coefficient 0.2.

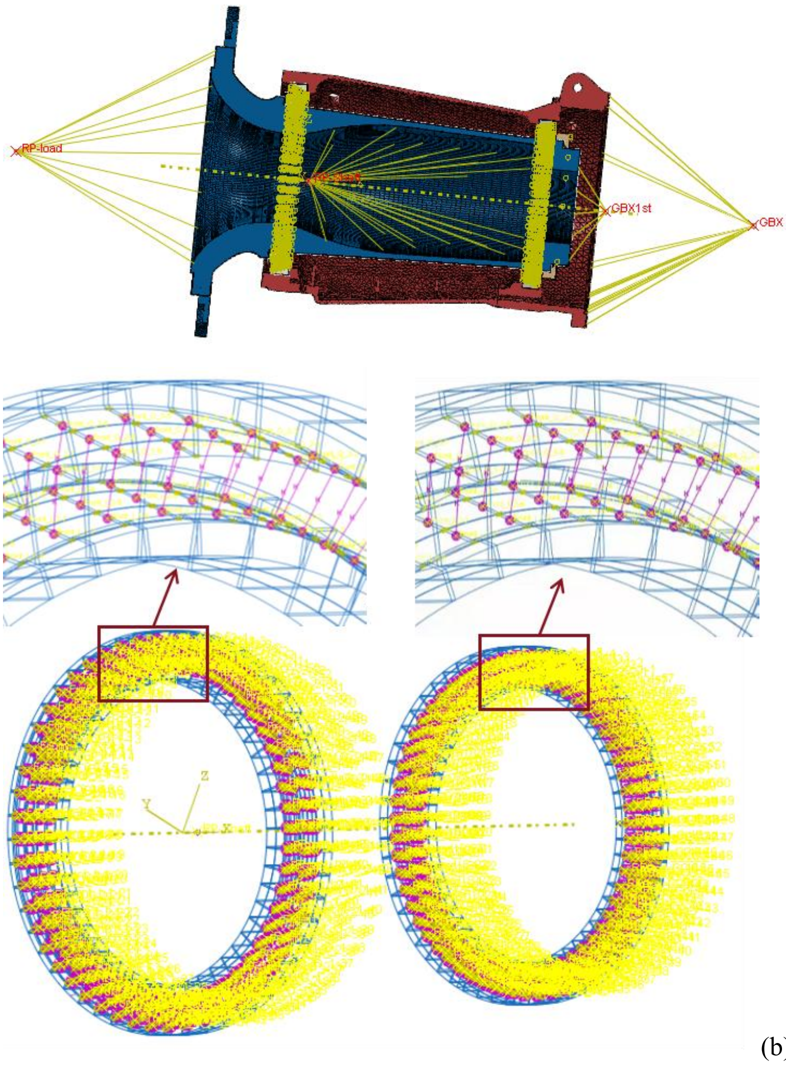

(a)

(b)

Fig 9. (a) Bearing system model, section view; (b) TRB models.

https://doi.org/10.5194/wes-2025-70
Preprint. Discussion started: 5 May 2025

eawe european academy of wind energy
Open Access WIND ENERGY SCIENCE DISCUSSIONS

Tow typical load cases shown in Table 3 are analyzed. These loads are expressed according to coordinates in Fig. 3.

Table 3. Load cases to be analyzed

Load Cases	M_{YN} kNm	M_{ZN} kNm	F_{XN} kN	F_{YN} kN	F_{ZN} kN
LAC1	-20910	217	241	65	-1711
LAC2	-15055	16546	184	56	-1723
Main shaft weight: 22000kg; Gear box 1st planetary stage weight: 12050kg; Gear box weight excluding 1st planetary stage: 28700kg.					

4.2 Results and discussion

As an example, Fig. 10 illustrates the deformation of the entire system under LAC2, while Fig. 11 presents the load distribution. The load distribution results obtained with rigid model and FEA model presented in the paper are listed together for comparison.

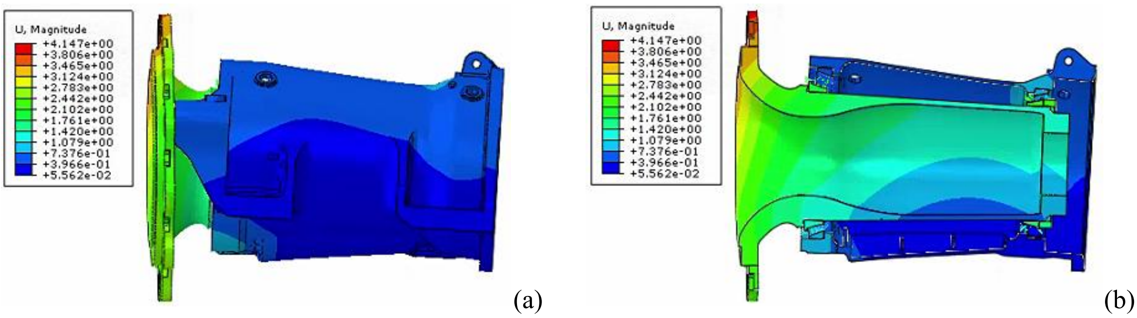

Fig 10. Bearing system deformation (scale factor 50) (a) overall view; (b) section view.

It is evident that due to the deformation of the main shaft and the bearing housing, more rollers are subjected to load. This indicates a slightly more uniform load distribution comparing to the rigid model, with the maximum raceway load in the FEA being decreased by about 25% compared to the rigid model shown in Fig. 11(a). However, the bearing housing feet cause an increase in load at stiffness hard points. The bearing radial load always points towards the position of the maximum load in the rigid model load distribution. When the radial load points towards the bearing housing foot, the maximum raceway load increases sharply, and it can even exceed the results of the rigid model, as shown in Fig. 11(b).

https://doi.org/10.5194/wes-2025-70
Preprint. Discussion started: 5 May 2025

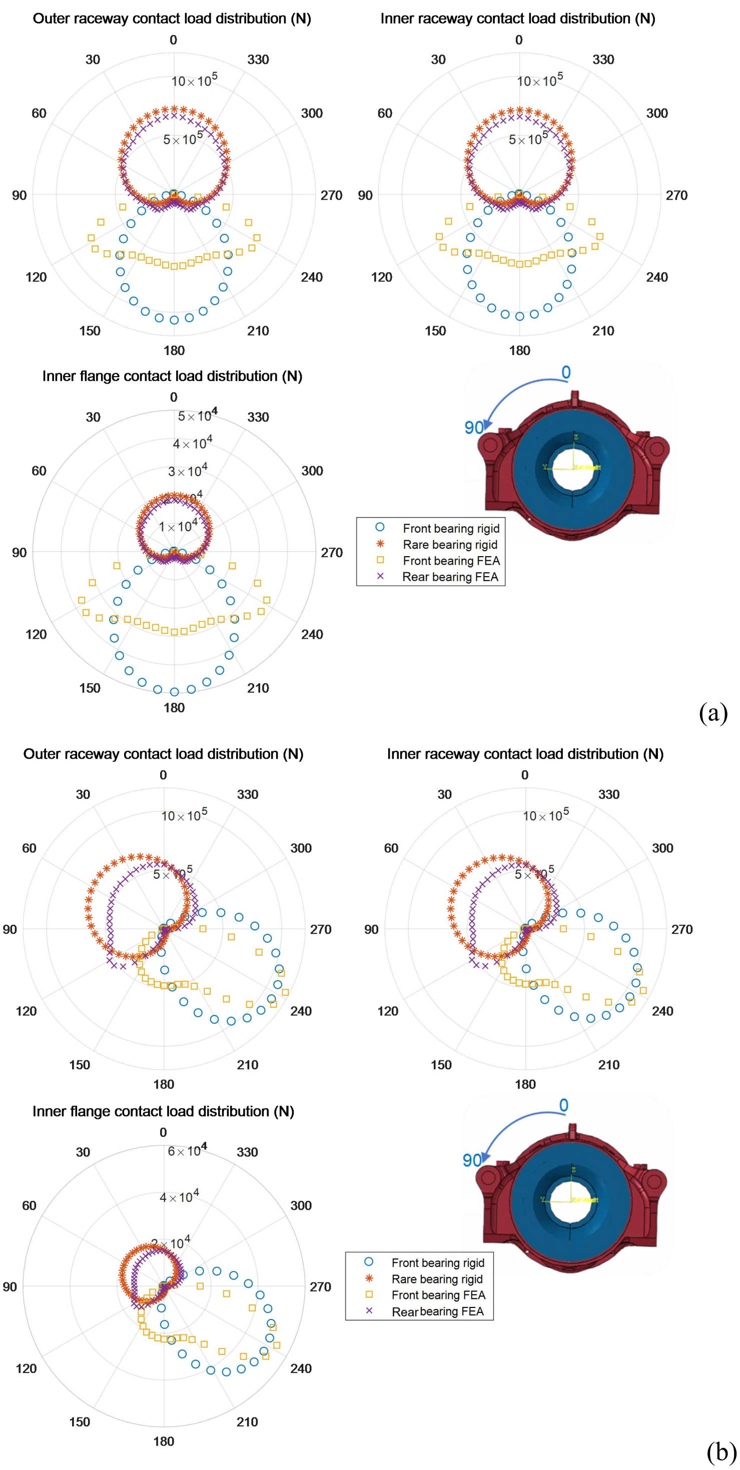

170 **Fig 11. Load distribution on raceways and inner flange: (a) LAC1; (b) LAC2.**

https://doi.org/10.5194/wes-2025-70
Preprint. Discussion started: 5 May 2025

Bearing rings can deform together with the whole bearing system. Taking the front bearing as an example, Fig. 12(a) shows a section view of the deformed front bearing under LAC2, and it shows the tilting between inner raceway and outer raceway, which would be significant to roller profile modification. Arbitrarily pick four nodes on bearing outer and inner raceways respectively at the maximum loaded section as shown in Fig. 12(b), then raceways can be expressed by vector AB and CD. The tilting angle between the two raceways is determined to be 0.02° according to Eq. (12). The contact pressure along the profiled roller can be solved by the lamina method, which is discussed in many references (Tedric A. Harris & Kotzalas, 不详-a) and will not be repeated in the paper. Considering the profile shown in Eq. (13), the influence of tilting angle on the contact pressure along the maximum load roller is shown in Fig. 13, and it shows that the tilting angle influences the contact pressure significantly.

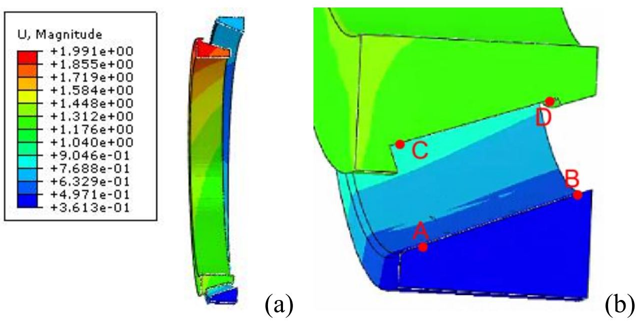

Fig 12. Front bearing deformation: (a) section view with scale factor 50, (b) local section view at maximum contact load region.

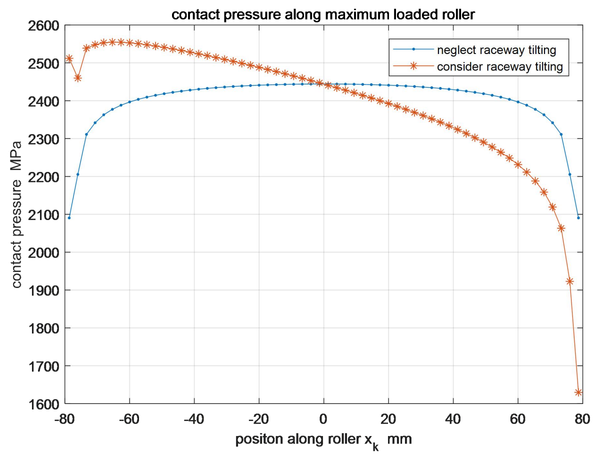

Fig 13. Contact pressure along the roller

$$\theta = \text{acos}\left(\frac{AB \cdot CD}{|AB||CD|}\right) \tag{12}$$

$$P(x_k) = 0.0003D_{\text{we}}\ln\left[\frac{1}{1-(2x_k/L_{\text{we}})^2}\right] \tag{13}$$

where, x_k: x coordinate along the roller of the k^{th} lamina (mm); $P(x_k)$: radius reduction at x_k position (mm).

Conclusions

The paper developed a TRB raceway contact load model based on the rigid assumption of the bearing system, taking the pre-tightening amount into consideration.

A TRB FEA model that incorporates system deformation effects is proposed and validated through a wind turbine main bearing system case. By replacing rollers with spring-based elements aligned with the outer raceway geometry, the proposed model effectively captures contact load distributions while bypassing the computational challenges of traditional solid-element roller modeling. Validation against a detailed solid-element model demonstrated excellent agreement in reaction forces and deformation results, with the spring model achieving a 99.7% reduction in computational time (103.7s vs. 37,539s), enabling rapid analysis of large-scale bearing systems.

Application to a wind turbine TRB+TRB main bearing system revealed that system deformation significantly alters load distribution compared to rigid assumptions. While deformation generally promotes more uniform load sharing among rollers, localized stiffness variations, such as bearing housing feet, can amplify peak loads by up to 25%, particularly when radial loads align with structural hardpoints. Additionally, tilting between inner and outer raceways (e.g., 0.02° in the front bearing under LAC2) was shown to critically influence contact pressure profiles along profiled rollers, underscoring the necessity of incorporating system deformation in TRB design optimization.

References

Nie Xinyu, Wang Xiaofang, Liu Yong, et al., (2023). Simulation of wind turbine main shaft strength based on meshless method. Mechanical & Electrical Engineering, *40*(11), 1760–1767.

Gao, X. H., Huang, X. D., Wang, H., & Chen, J. (2011). Modelling of ballraceway contacts in a slewing bearing with non-linear springs. *Proceedings of the Institution of Mechanical Engineers, Part C: Journal of Mechanical Engineering Science*, *225*(4), 827–831. https://doi.org/10.1177/09544062JMES2454

Gao, X., & Zhang, Z. (2024). A simplified spherical roller bearing model and its application in the wind turbine main bearing system finite element modeling. *Tribology International*, *196*, 109678. https://doi.org/10.1016/j.triboint.2024.109678

Germanischer Lloyd. (2010). *Guideline for the Certification of Wind Turbines*. Germanischer Lloyd.

Gunia, D., & Smolnicki, T. (2017). The Analysis of the Stress Distribution in Contact Pairs Ball-Wire and Wire-Ring in Wire Raceway Slewing Bearing. E. Rusiński & D. Pietrusiak, *Proceedings of the 13th International Scientific Conference* (页 185–195). Springer International Publishing. https://doi.org/10.1007/978-3-319-50938-9_20

He, P., Wang, Y., & Wang, H. (2021). An Analysis Method of Carrying Capacity Accuracy of Three-Row Roller Slewing Bearing. *Mechanics*, *27*(5), 360–367. https://doi.org/10.5755/j02.mech.28111

Krynke, M., Kania, L., & Mazanek, E. (2011). Modelling the Contact between the Rolling Elements and the Raceways of Bulky Slewing Bearings. *Key Engineering Materials*, *490*, 166–178. https://doi.org/10.4028/www.scientific.net/KEM.490.166

Liu, R., Wang, H., Pang, B. T., Gao, X. H., & Zong, H. Y. (2018). Load Distribution Calculation of a four-Point-Contact Slewing Bearing and its Experimental Verification. *Experimental Techniques*, *42*(3), 243–252. https://doi.org/10.1007/s40799-018-0237-2

https://doi.org/10.5194/wes-2025-70
Preprint. Discussion started: 5 May 2025

Lostado, R., Martinez, R. F., & Mac Donald, B. J. (2015). Determination of the contact stresses in double-row tapered roller bearings using the finite element method, experimental analysis and analytical models. *Journal of Mechanical Science and Technology*, *29*(11), 4645–4656. https://doi.org/10.1007/s12206-015-1010-4

Lostado-Lorza, R., Escribano-Garcia, R., Fernandez-Martinez, R., Illera-cueva, M., & Mac Donald, B. J. (2017). Using the finite element method and data mining techniques as an alternative method to determine the maximum load capacity in tapered roller bearings. *Journal of Applied Logic*, *24*, 4–14. https://doi.org/10.1016/j.jal.2016.11.009

Safian, A., Wu, N., & Liang, X. (2021, June 27). Dynamic Simulation Of A Roller Bearing By Combining Finite Element And Lumped Parameter Models. *Progress in Canadian Mechanical Engineering. Volume 4*. Canadian Society for Mechanical Engineering International Congress (2021 : Charlottetown, PE). https://doi.org/10.32393/csme.2021.37

Stammler, M., Menck, O., Guo, Y., & Keller, J. (2024). *Wind Turbine Design Guideline DG03: Yaw and Pitch Bearings* (No. NREL/TP-5000-89161). NREL. https://www.nrel.gov/docs/fy24osti/89161.pdf

Tedric A. Harris, & Kotzalas, M. N. *Rolling Bearing Analysis—Advanced Concepts of Bearing Technology* (5th edition). Taylor & Francis.

Tedric A. Harris, & Kotzalas, M. N. *Rolling Bearing Analysis—Essential Concepts of Bearing Technology* (5th edition). Taylor & Francis.

Wang, H., He, P., Pang, B., & Gao, X. (2017). A new computational model of large three-row roller slewing bearings using nonlinear springs. *Proceedings of the Institution of Mechanical Engineers, Part C: Journal of Mechanical Engineering Science*, *231*(20), 3831–3839. https://doi.org/10.1177/0954406217704223

Yongqi, Z., Qingchang, T., Kuo, Z., & Jiangang, L. (2012). Analysis of Stress and Strain of the Rolling Bearing by FEA method. *Physics Procedia*, *24*, 19–24. https://doi.org/10.1016/j.phpro.2012.02.004